Supporting information for

Achieving near-infrared emission in platinum (II) complexes by using an extended donor-acceptor-type ligand

You-Ming Zhang,[a] Fanyuan Meng,[a,b] Jian-Hong Tang,[c] Yafei Wang,[a] Caifa You,[a] Hua Tan,[a] Yu Liu,[a] Yu-Wu Zhong,[d,*] Shijian Su,[c*] and Weiguo Zhu[a, b*]

[a] *College of Chemistry, Xiangtan University, Key Lab of Environment-Friendly Chemistry and Application in Ministry of Education, Xiangtan 411105, China.*

[b] *School of Materials Science and Engineering, Changzhou University, Changzhou 213164, China*

[c] *Institute of Polymer Optoelectronic Materials and Devices, State Key Laboratory of Luminescent Materials and Devices, South China University of Technology, Guangzhou 510640, China.*

[d] *Beijing National Laboratory for Molecular Sciences, CAS Key Laboratory of Photochemistry, Institute of Chemistry, Chinese Academy of Sciences, Beijing 100190, China.*

Email addresses:

(W. Z) zhuwg18@126.com,

(S. S) mssjsu@scut.edu.cn,

(Y.-W.Z.) zhongyuwu@iccas.ac.cn

1. General considerations for characterization

1.1. Instrument

Nuclear magnetic resonance (NMR) spectra were recorded on a Bruker DRX 400 spectrometer using tetramethylsilane as a reference in deuterated chloroform solution at 298 K. MALDI-TOF mass spectrometric measurements were performed on Bruker Bifiex III MALDI-TOF. Thermogravimetric analysis (TGA) was conducted under a dry nitrogen gas flow at a heating rate of 10 ^{o}C min^{-1} on a Perkin-Elmer TGA 7. UV-Vis absorption spectra were recorded on a HP-8453 UV visible system. UV/vis/ NIR spectra were recorded using a PE Lambda 750 UV/vis/NIR spectrophotometer. Cyclic voltammetry was carried out on a CHI660A electrochemical work station in a three-electrode cell dipped in a 0.1 mol L^{-1} tetrabutylammonium hexafluorophosphate (Bu_4NPF_6) acetonetrile solution under nitrogen protection at a scan rate of 100 mV s^{-1} and room temperature (RT). In this three-electrode cell, a platinum rod, platinum wire and saturated calomel electrode were used as a working electrode, counter electrode and reference electrode, respectively.

2.2 PLEDs Fabrication

The single-emissive-layer (SEL) PLEDs using $[Fl(TPA\text{-}BTPy)_2]Pt_2(pic)_2$ as dopant were fabricated by spin-coating and vacuum thermal evaporation. The device configuration is ITO/ PEDOT:PSS, 40 nm/ PVK-30 wt% OXD-7: dopant, 80 nm/Ba, 4 nm/Al, 100 nm, where indium tin oxide (ITO) acts as the anode, poly(3,4-ethylene dioxy-thiophene):poly(styrenesulfonate) (PEDOT: PSS) is used as an anode buffer layer at the interface of ITO, Ba and Al are employed as electron injection layer and cathode layer, respectively. The light-emitting layer consists of PVK, OXD-7 and

dopant, where PVK acts as the host material due to its excellent film-forming and hole-transporting properties. To facilitate electron transport in the light-emitting layer, OXD-7 is simultaneously mixed with PVK. The weight ratio of PVK and OXD-7 is 70:30 (*W/W*). The dopant concentrations vary from 1.0 wt % to 3.0 wt %.

Table S1. Calculated excitation energy (E), oscillator strength (f), dominant contributing transitions and associated percent contribution and assignment of complex [Fl(TPA-BTPy)$_2$]Pt$_2$(pic)$_2$.[a]

Compounds	S_n	*E*/ eV	*E*/ nm	*f*	Dominant transitions (percent contribution[b])	assignment
[Fl(TPA-BTPy)$_2$]Pt$_2$(pic)$_2$	2	2.04	607	0.13	HOMO→LUMO (50.5%)	ILCT
					HOMO→LUMO+1 (48.5%)	ILCT
	3	2.11	587	0.52	HOMO-1→LUMO (95.0%)	ILCT
	4	2.53	490	0.06	HOMO-1→LUMO+1(91.9%)	ILCT
	5	2.58	479	0.21	HOMO-2→LUMO (59.7%)	ILCT
					HOMO-3→LUMO (26.1%)	ILCT
	6	2.62	474	0.003	HOMO→LUMO+2 (97.5%)	LLCT
	7	2.66	467	0.00056	HOMO→LUMO+4 (95.6%)	LLCT
	10	2.71	458	0.16	HOMO→LUMO+3 (83.0%)	ILCT/MLCT
	12	2.89	428	0.002	HOMO-4→LUMO+1 (86.5%)	MLCT
	15	2.97	417	0.36	HOMO-1→LUMO+3 (69.5%)	ILCT/LLCT
	16	3.03	409	0.12	HOMO-5→LUMO+1 (44.8%)	LLCT
					HOMO-3→LUMO+1 (21.6%)	ILCT
					HOMO-2→LUMO+1 (10.1%)	ILCT
	21	3.18	390	0.0013	HOMO-1→LUMO+4 (88.8%)	ILCT/LLCT
					HOMO-1→LUMO+3 (4.7%)	ILCT/LLCT
	23	3.27	379	0.026	HOMO-1→LUMO+5 (22.3%)	ILCT/LMCT
					HOMO-2→LUMO+4 (22.1%)	ILCT/LLCT
	26	3.28	377	0.03	HOMO-1→LUMO+5 (34.5%)	ILCT/LLCT
					HOMO-3→LUMO+6 (15.8%)	ILCT/LLCT
					HOMO-2→LUMO+4 (13.6%)	LLCT
	29	3.34	370	0.242	HOMO-2→LUMO+3 (15.3%)	ILCT/LLCT
					HOMO-1→LUMO+6 (10.3%)	ILCT/LLCT
	31	3.36	367	0.011	HOMO-2→LUMO+2 (35.6%)	LLCT
					HOMO-3→LUMO+2 (13.8%)	LLCT
	37	3.44	360	0.035	HOMO-4→LUMO+4 (20.1%)	MLCT
	40	3.46	358	0.0067	HOMO-4→LUMO+4 (42.8%)	MLCT

[a] Computed at the TDDFT/B3LYP/LANL2DZ/6-31G*/CPCM. [b] The actual percent contribution =(configuration coefficient)^2×2×100%.

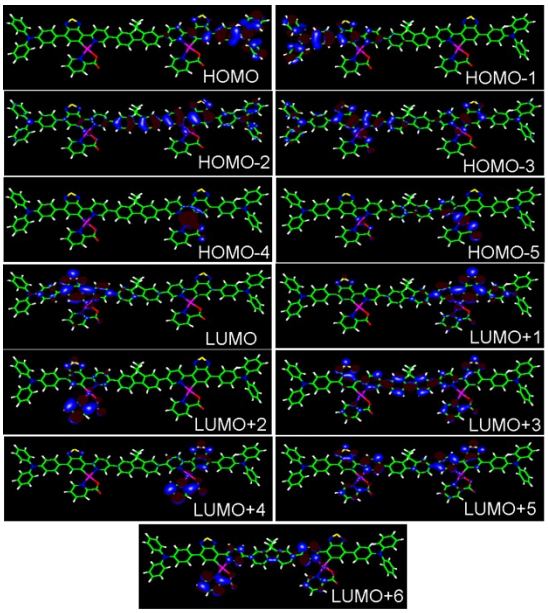

Figure S1. Isodensity plots of frontiers orbitals of $[Fl(TPA\text{-}BTPy)_2]Pt_2(pic)_2$. All orbitals have been computed at an isovalue of 0.03.

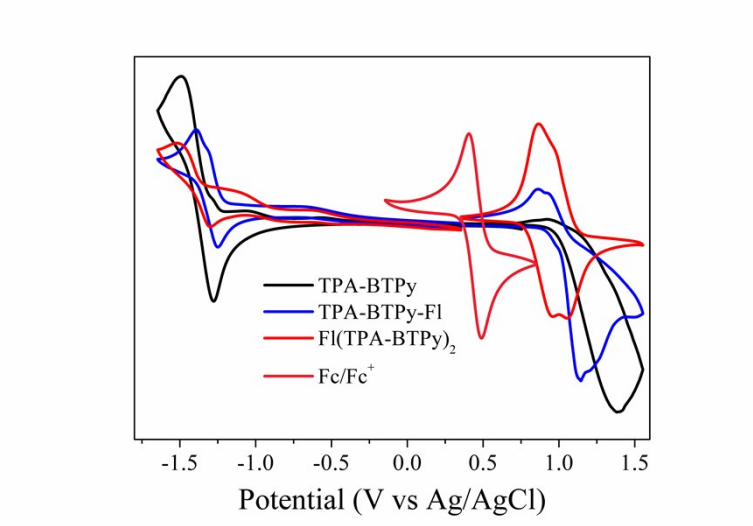

Figure S2. Cyclic voltammograms of the TPA-BTPy, TPA-BTPy-Fl and $Fl(TPA\text{-}BTPy)_2$ films on platinum electrode in acetonitrile solution containing 0.1 mol L^{-1} Bu_4NPF_6 at a scan rate of 100 mV s^{-1} .

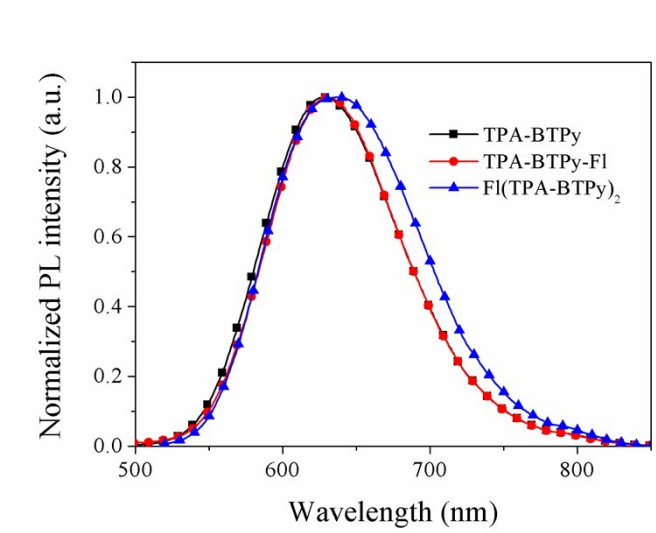

Figure S3. Normalized PL spectra of TPA-BTPy, TPA-BTPy-Fl, and Fl(TPA-BTPy)$_2$ in CH_2Cl_2 solution.

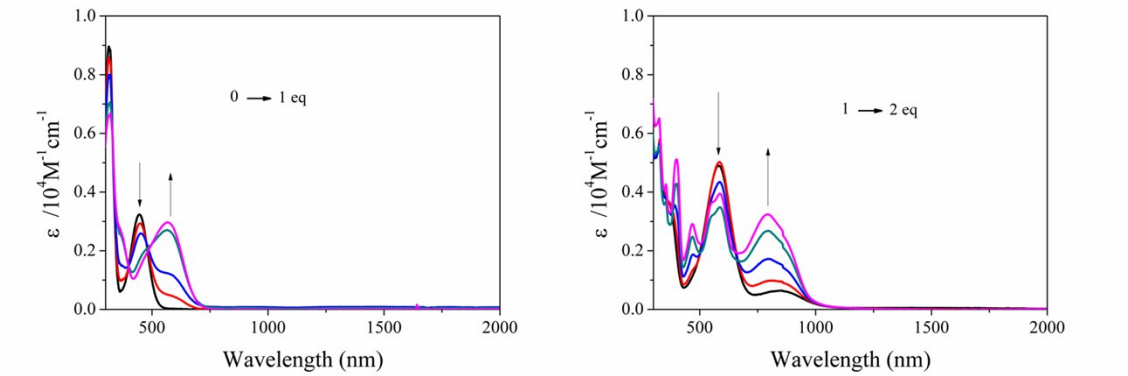

Figure S4. Absorption spectral changes of TPA-BTPy in DCM upon oxidation by the gradual addition of $SbCl_5$.

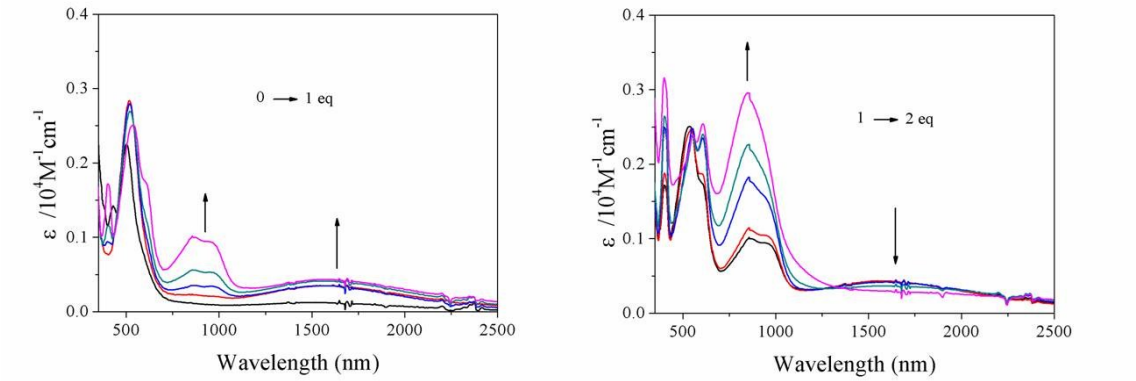

Figure S5. Absorption spectral changes of (TPA-BTPy)Pt(pic) in DCM upon oxidation by the gradual addition of $SbCl_5$.

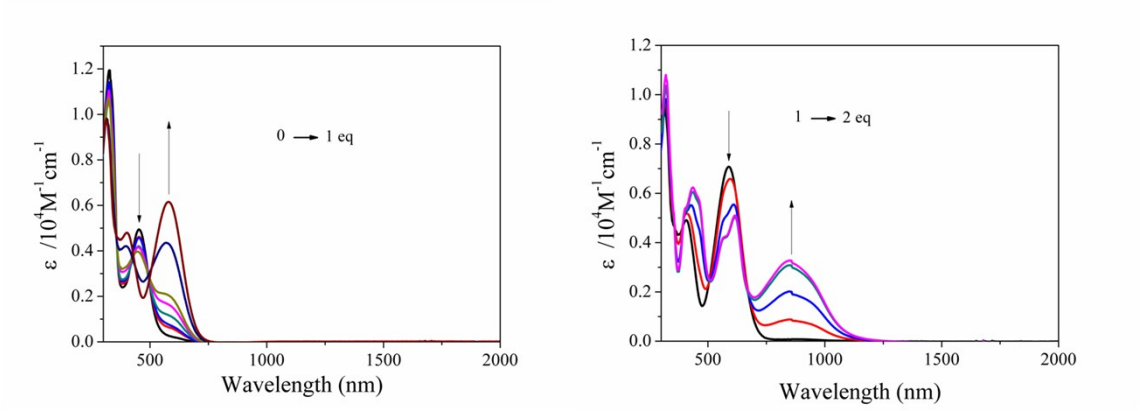

Figure S6. Absorption spectral changes of TPA-BTPy-Fl in DCM upon oxidation by the gradual addition of $SbCl_5$.

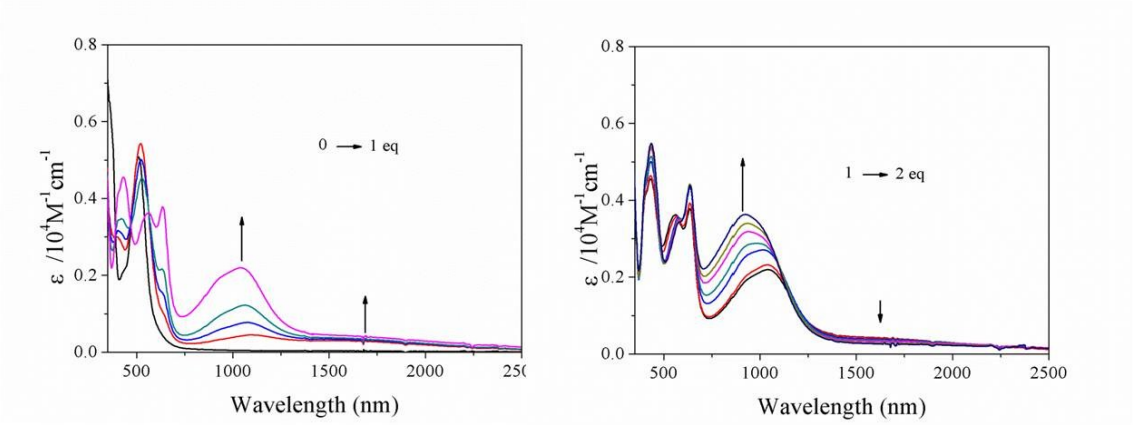

Figure S7. Absorption spectral changes of (TPA-BTPy-Fl)Pt(pic) in DCM upon oxidation by the gradual addition of $SbCl_5$.

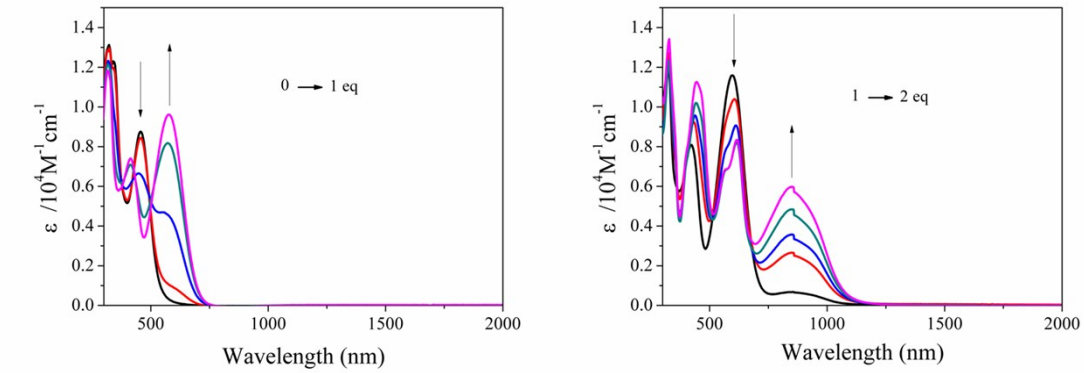

Figure S8. Absorption spectral changes of $Fl(TPA\text{-}BTPy)_2$ in DCM upon oxidation by the gradual addition of $SbCl_5$.

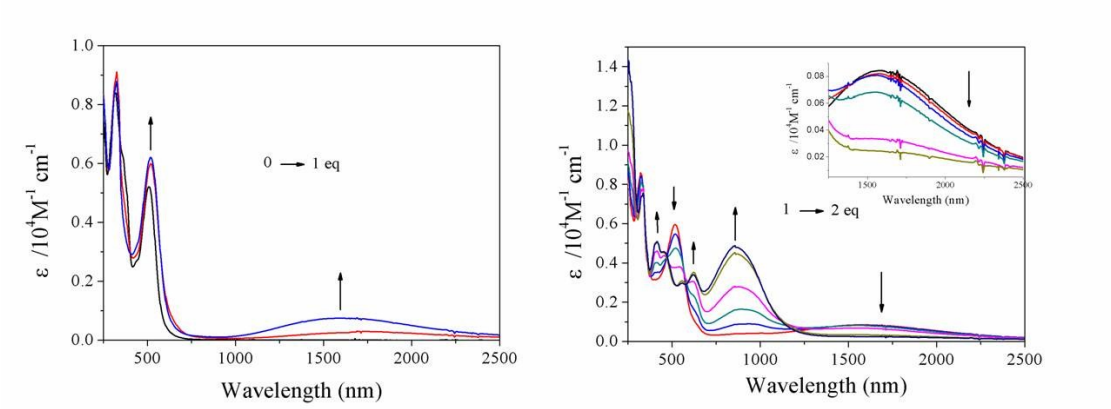

Figure S9. Absorption spectral changes of $[Fl(TPA\text{-}BTPy)_2]Pt_2(pic)_2$ in DCM upon oxidation by the gradual addition of $SbCl_5$.

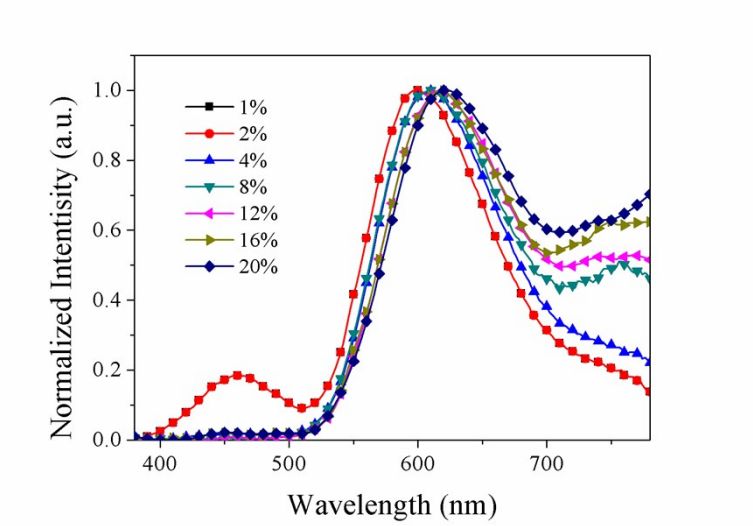

Figure S10. EL spectra of the $[Fl(TPA\text{-}BTPy)_2]Pt_2(pic)_2$-doped PLEDs at dopant concentrations from 1 to 20 wt%.

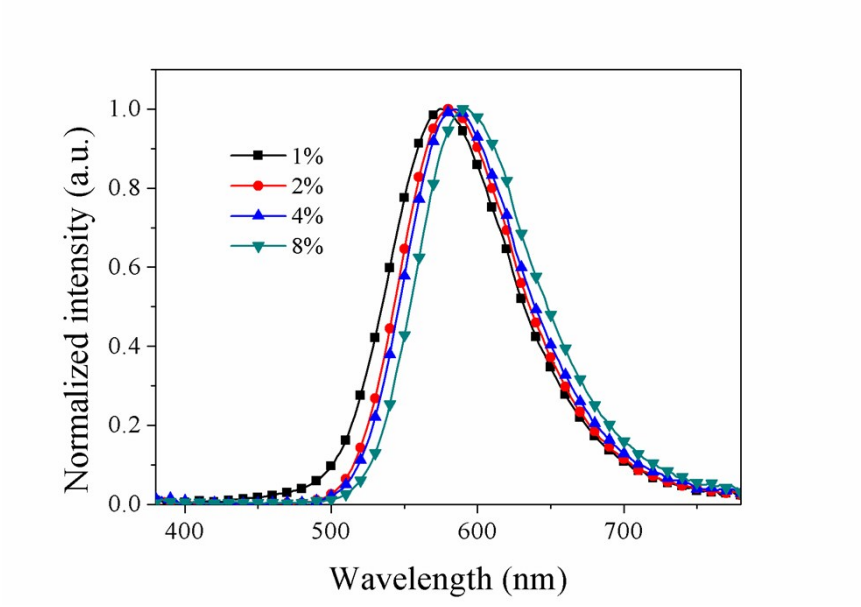

Figure S11. EL spectra of the Fl(TPA-BTPy)$_2$-doped PLEDs at dopant concentrations from 1 to 8 wt%.

^{1}H NMR plot of TPA-BT-Br

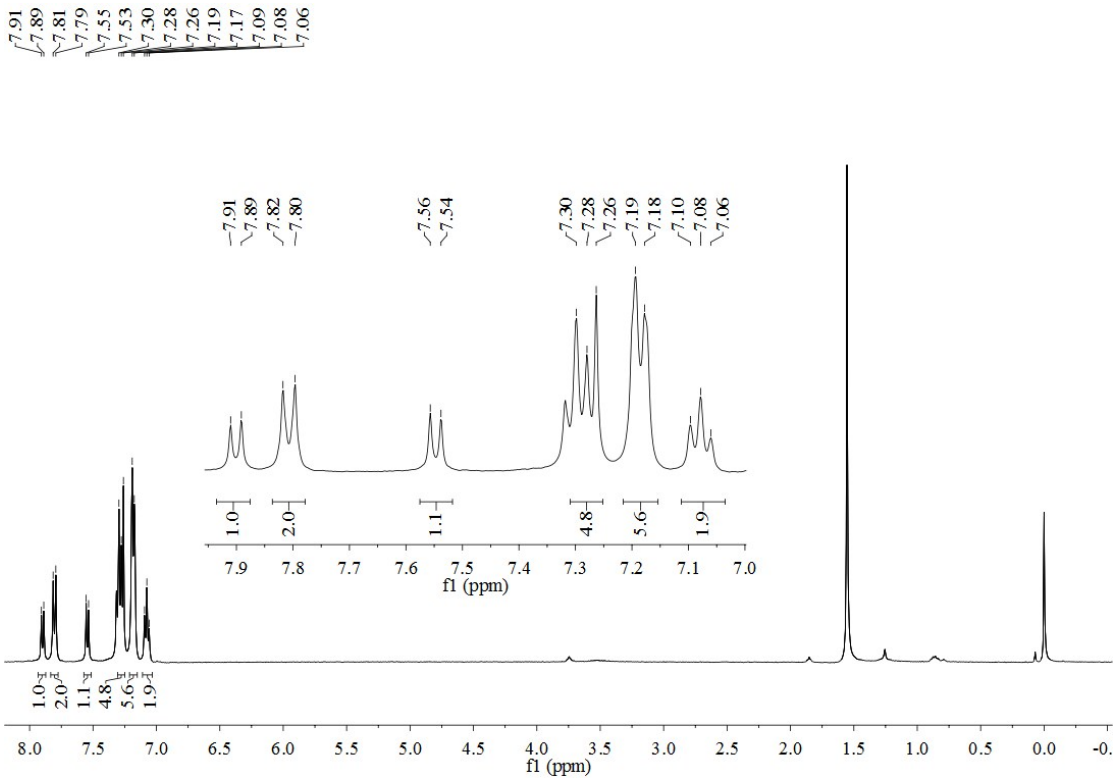

^{1}H NMR plot of TPA-BT-BPin

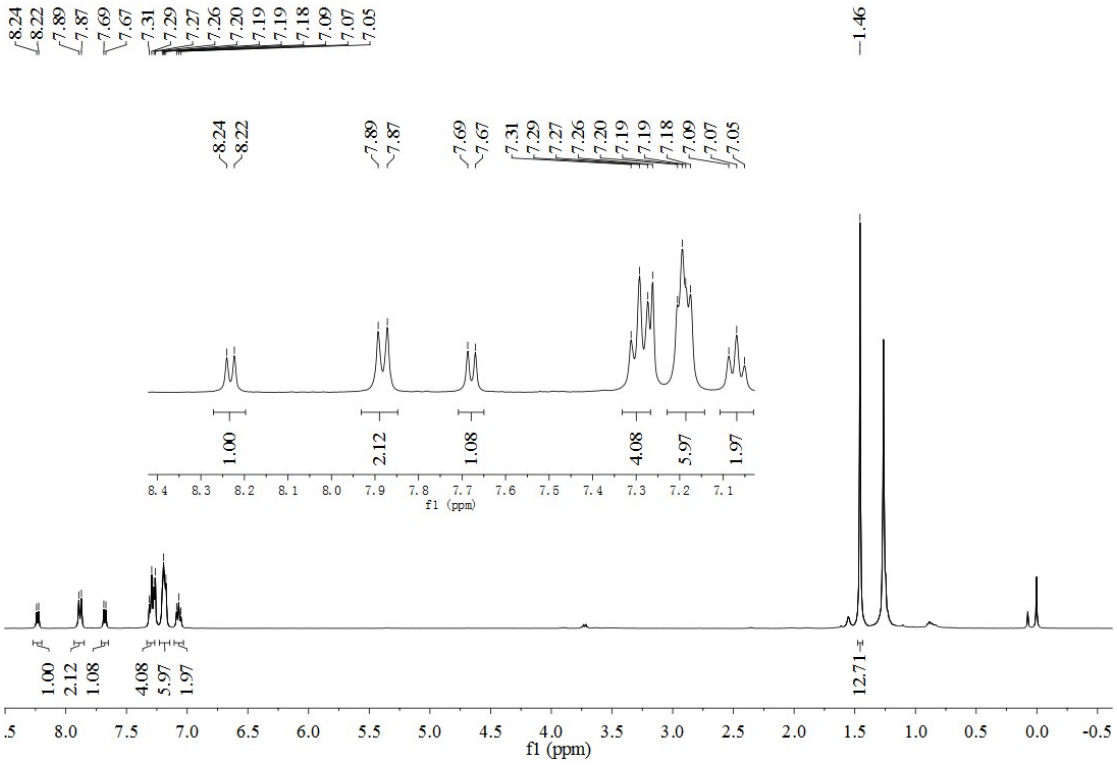

^{1}H NMR plot of TPA-BTpy

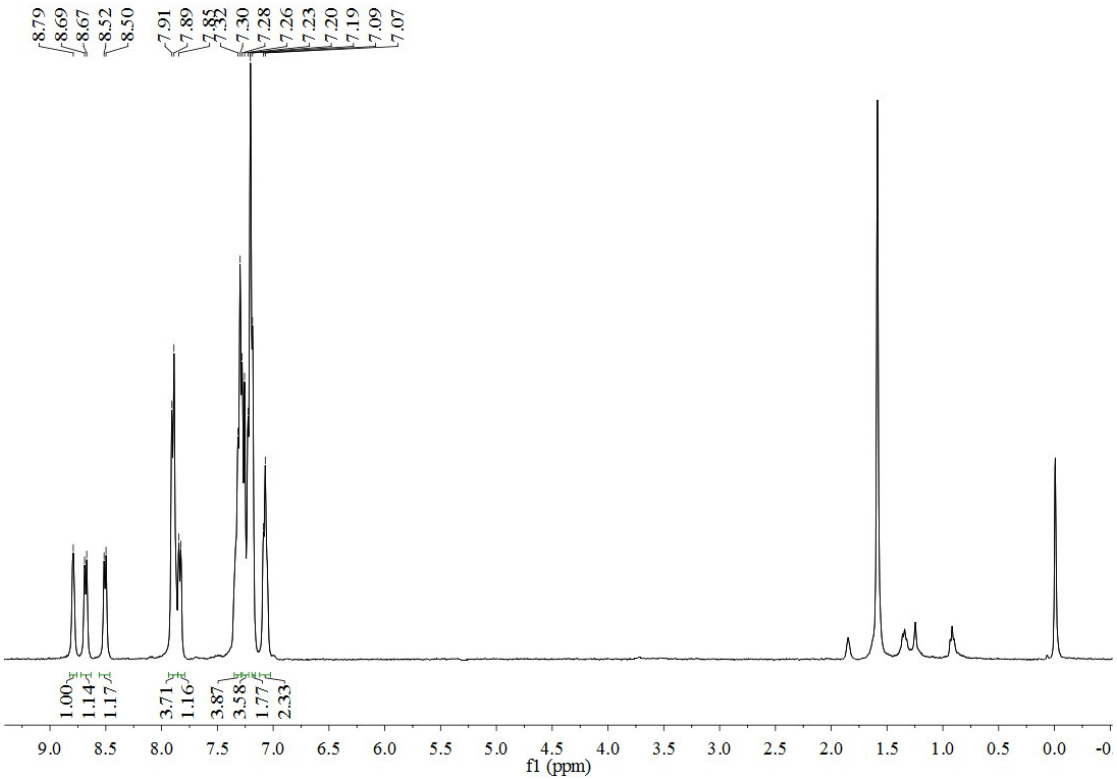

^{1}H NMR plot of TPA-BTPy-Br

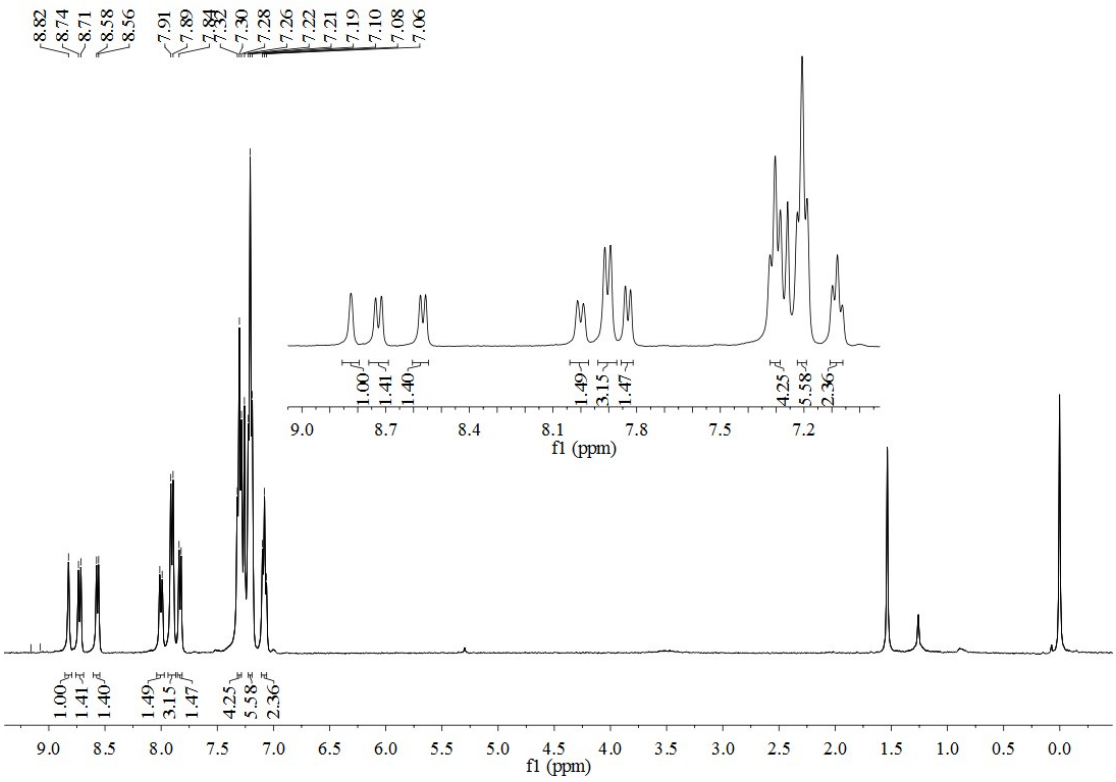

^{1}H NMR plot of TPA-BTPy-Fl

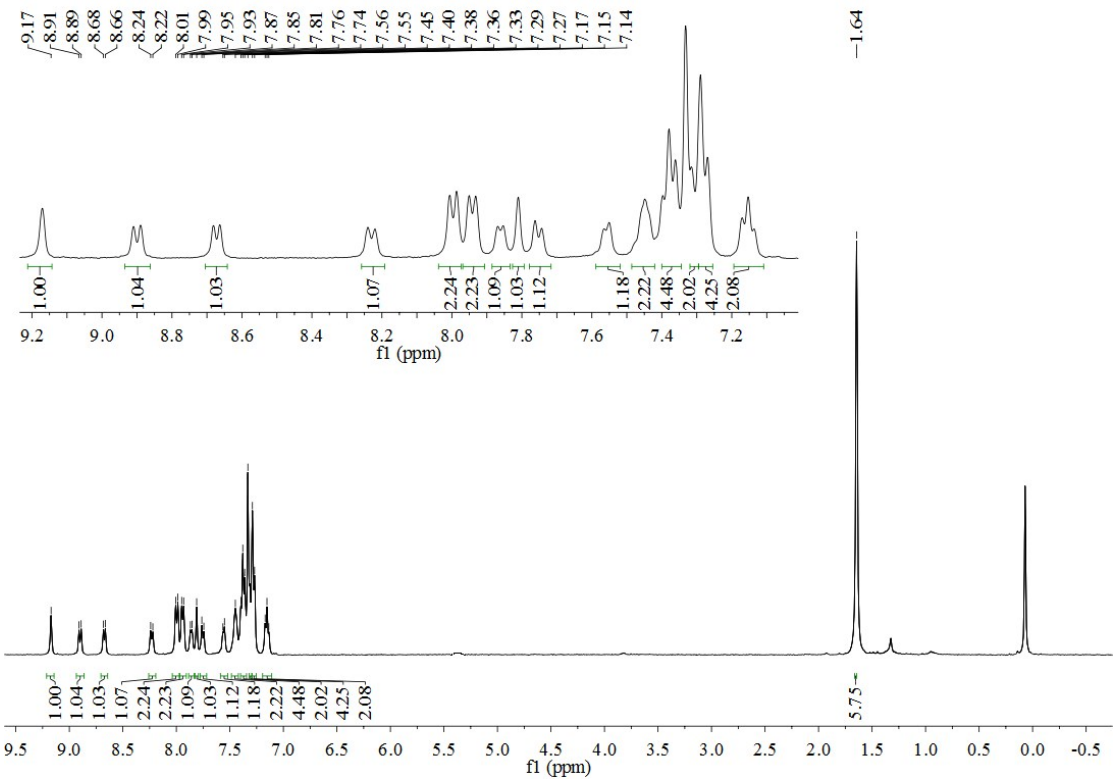

^{1}H NMR plot of Fl(TPA-BTPy)$_2$

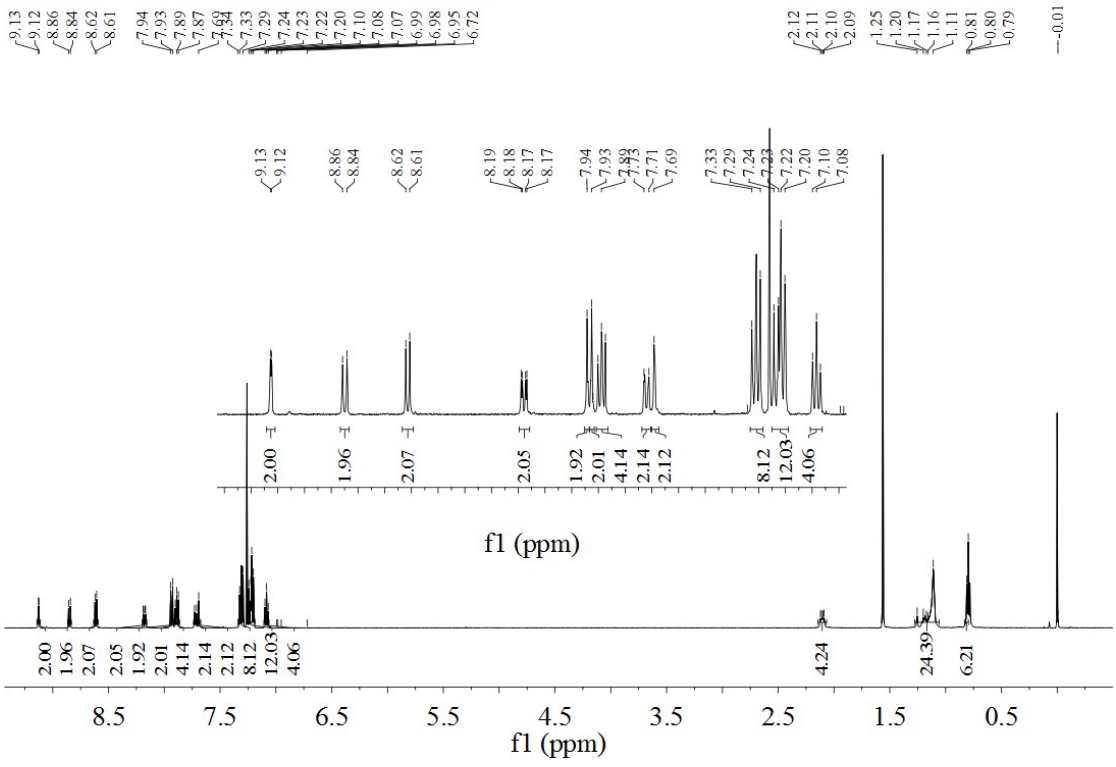

^{1}H NMR plot of (TPA-BTPy)Pt(pic)-Br

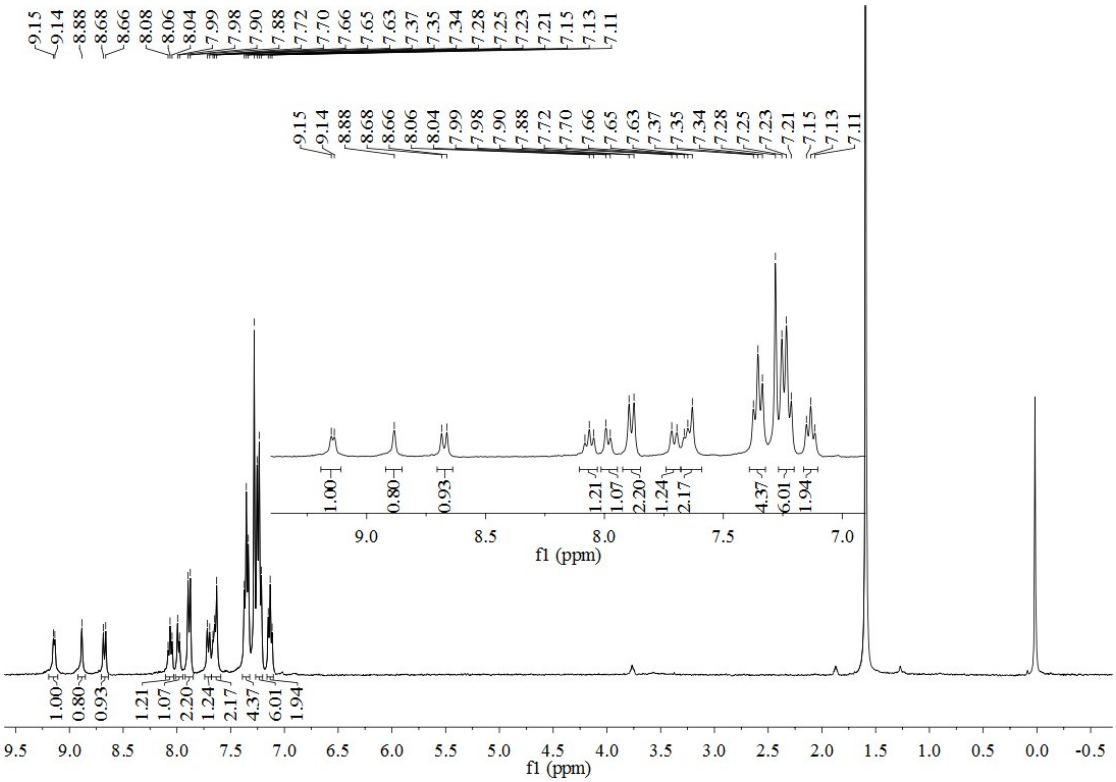

^{1}H NMR plot of (TPA-BTPy)Pt(pic)

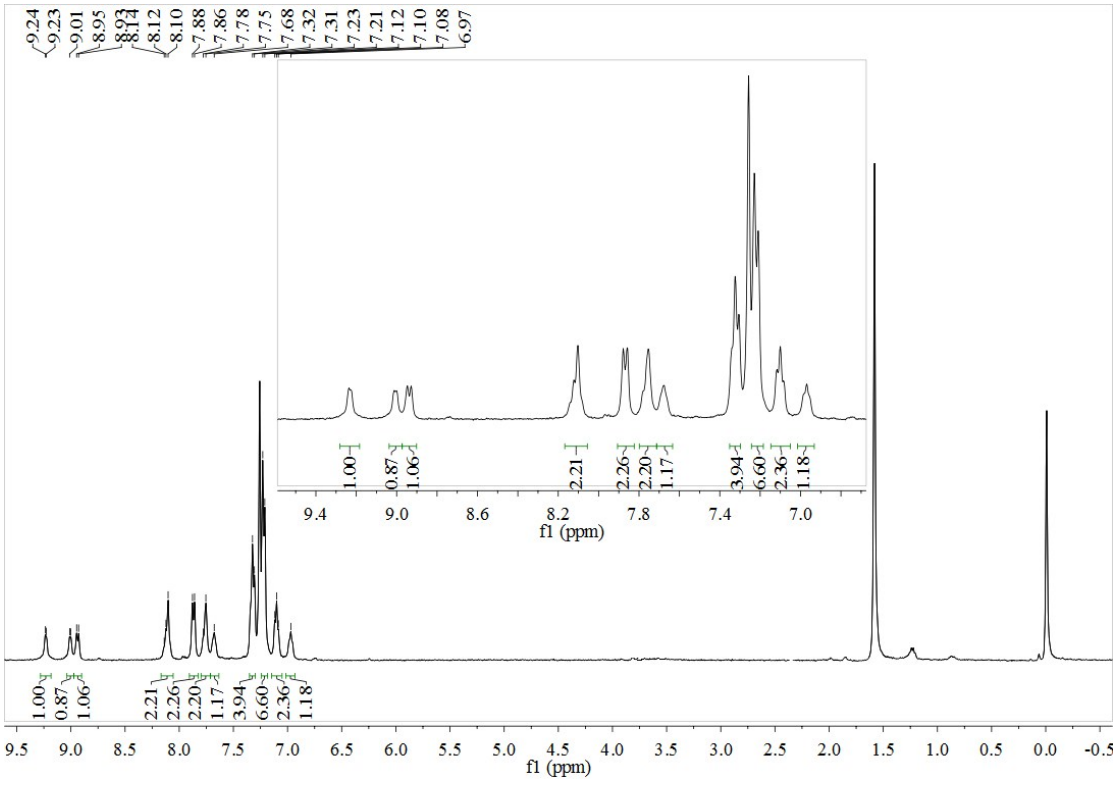

^{1}H NMR plot of (TPA-BTPy-Fl)Pt(pic)

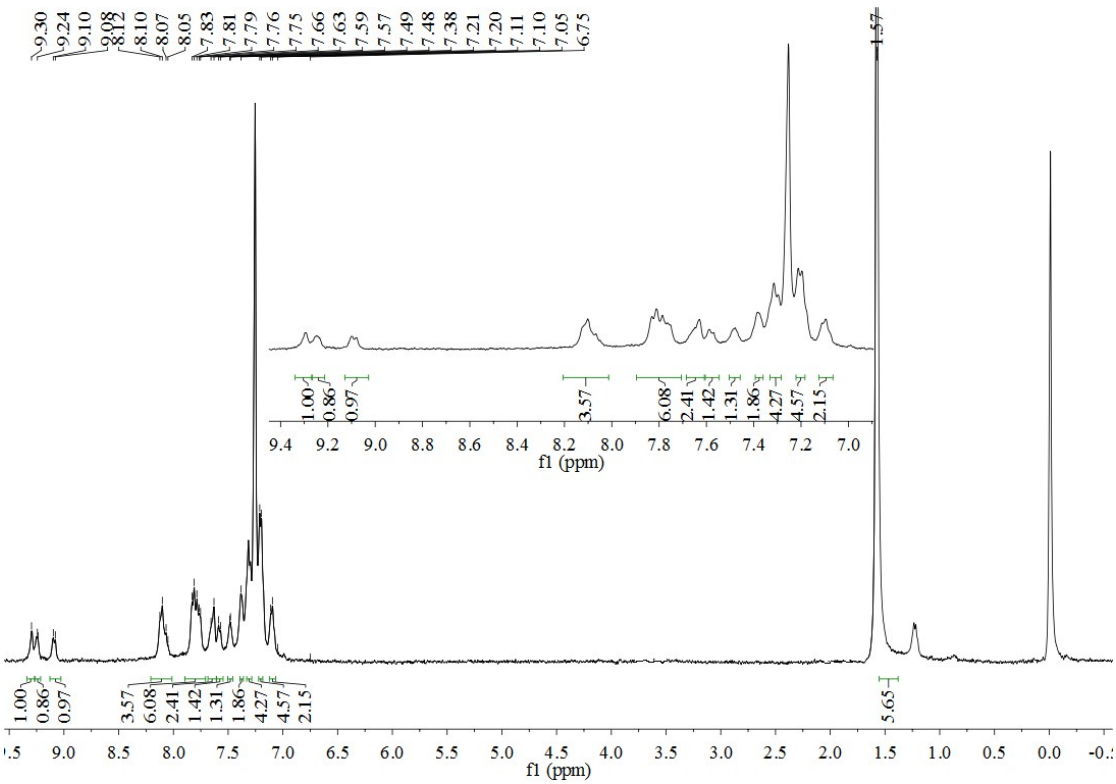

^{1}H NMR plot of [Fl(TPA-BTPy)$_2$]Pt$_2$(pic)$_2$

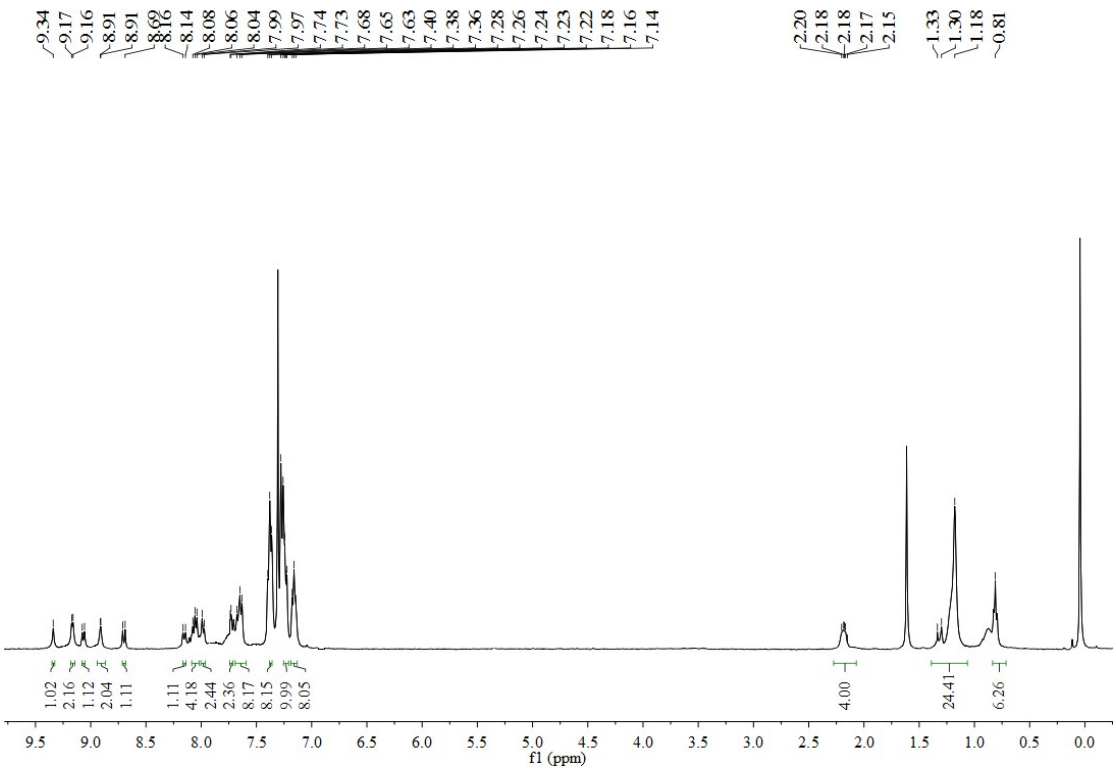

^{13}C NMR plot of TPA-BT-Br

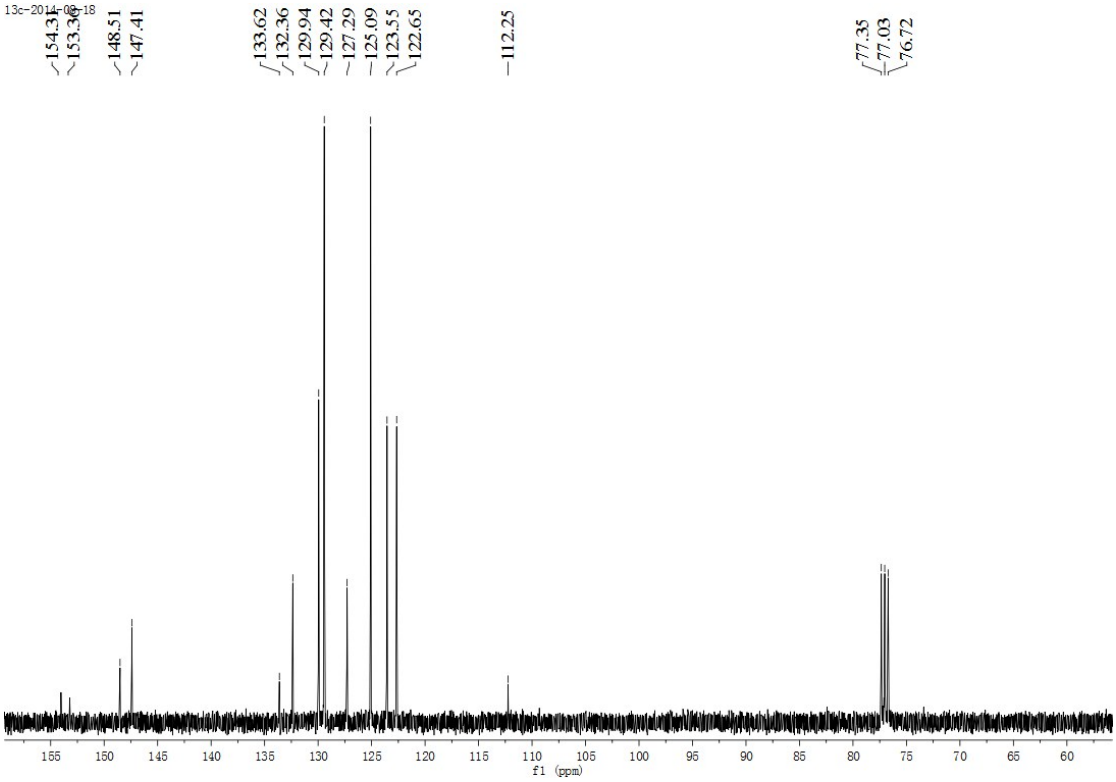

^{13}C NMR plot of TPA-BT-BPin

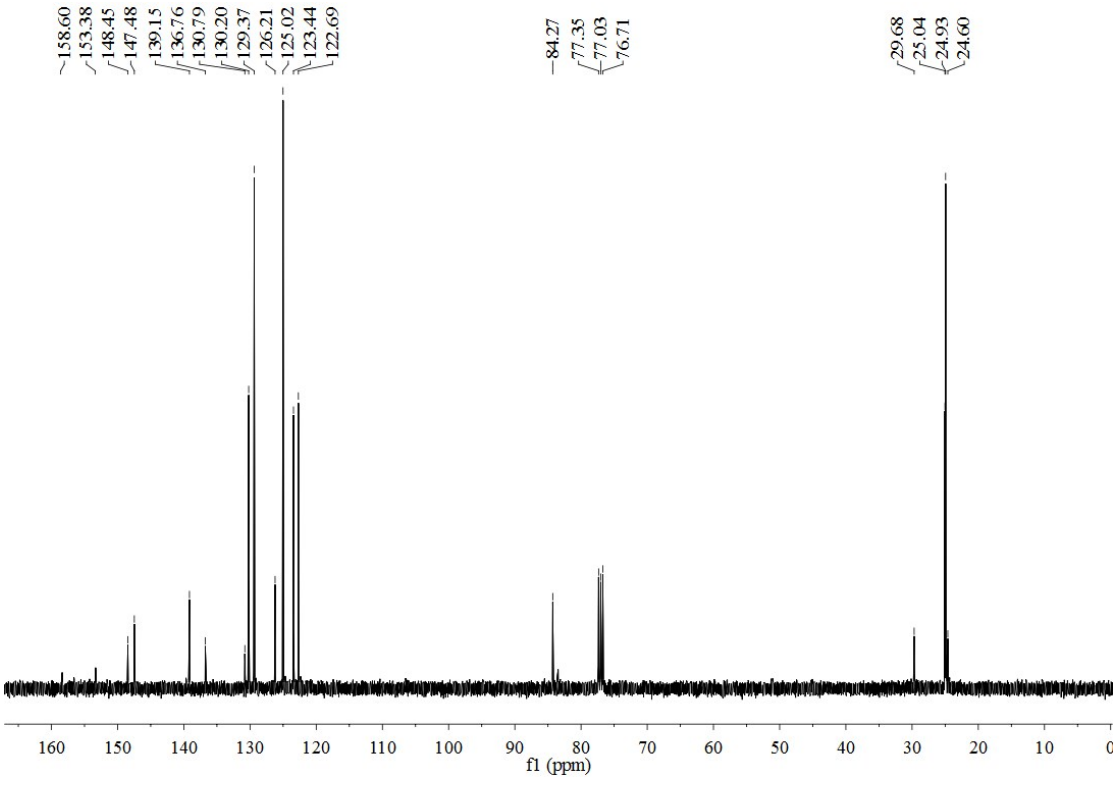

^{13}C NMR plot of TPA-BTPy

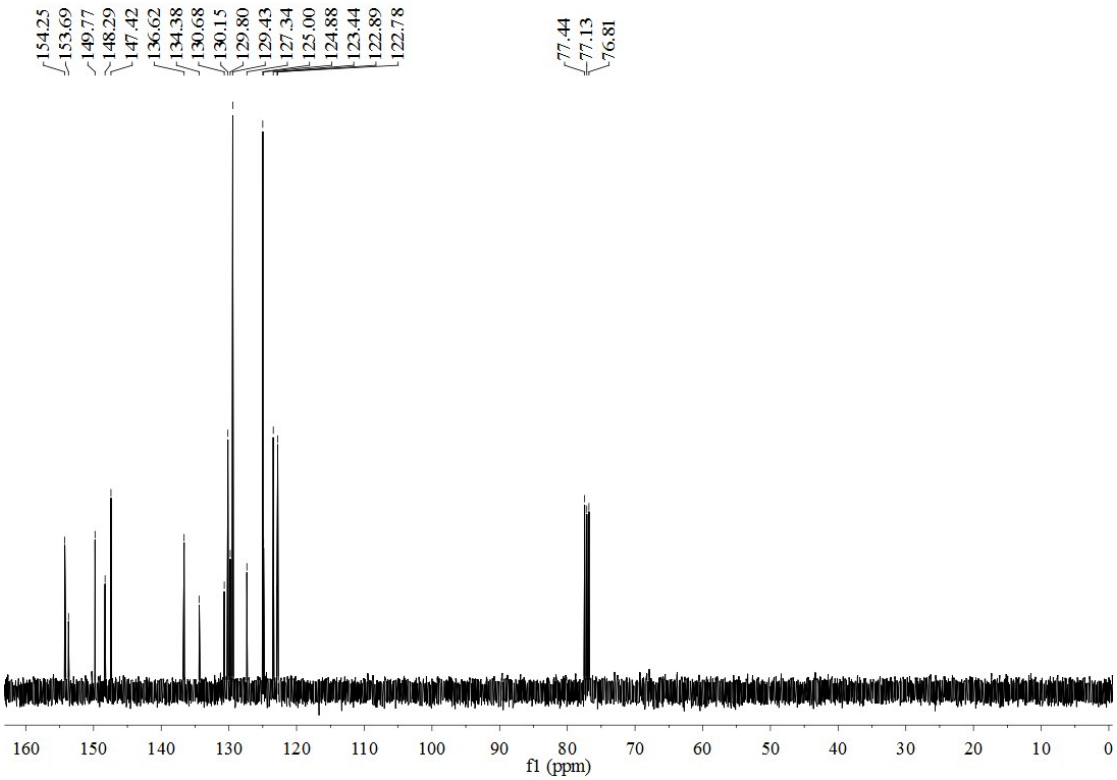

^{13}C NMR plot of TPA-BTPy-Br

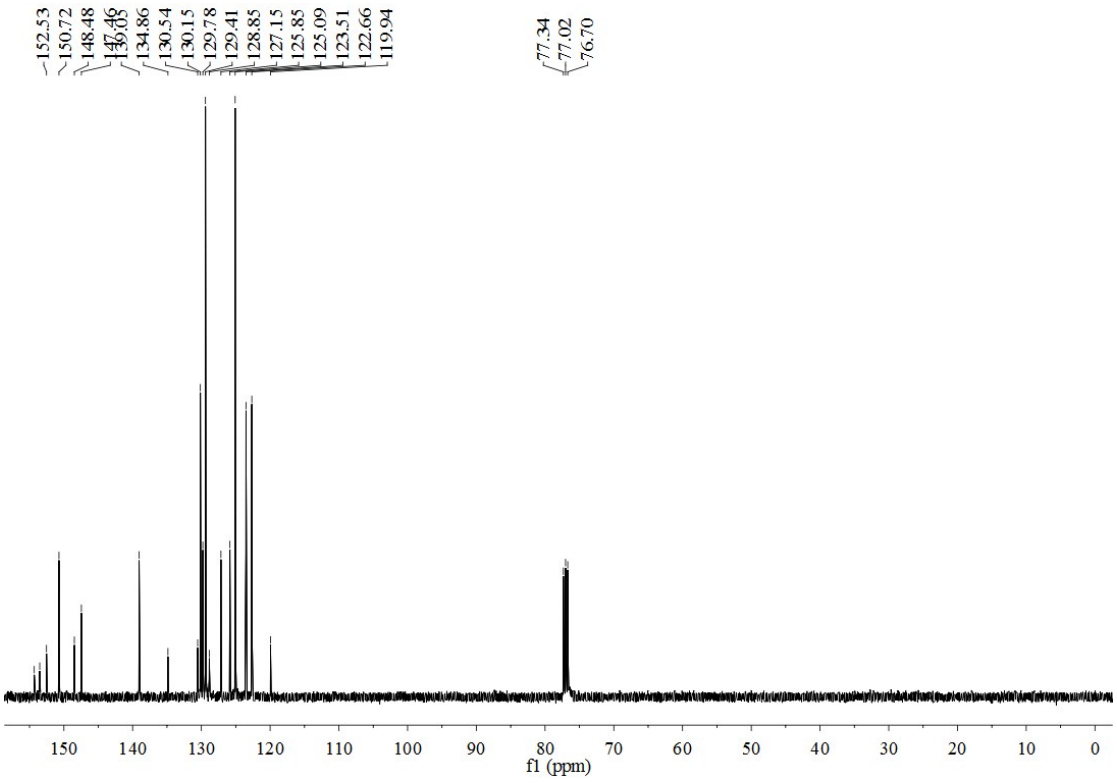

^{13}C NMR plot of TPA-BTPy-Fl

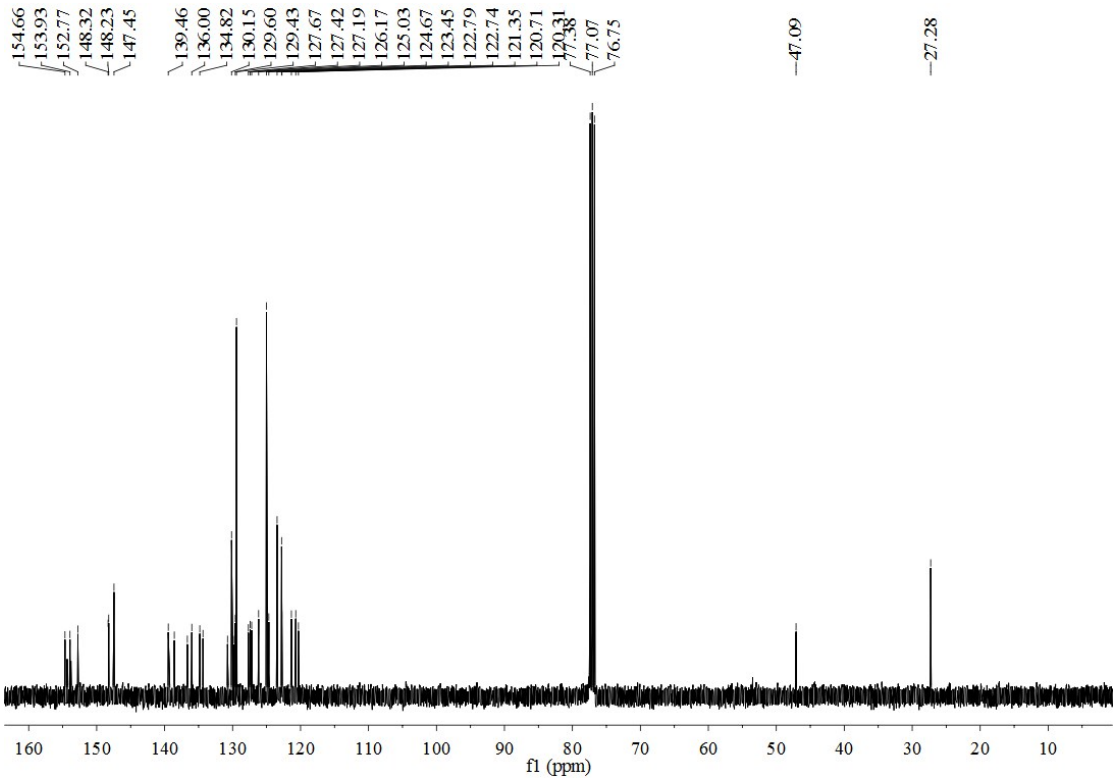

^{13}C NMR plot of Fl(TPA-BTPy)$_2$

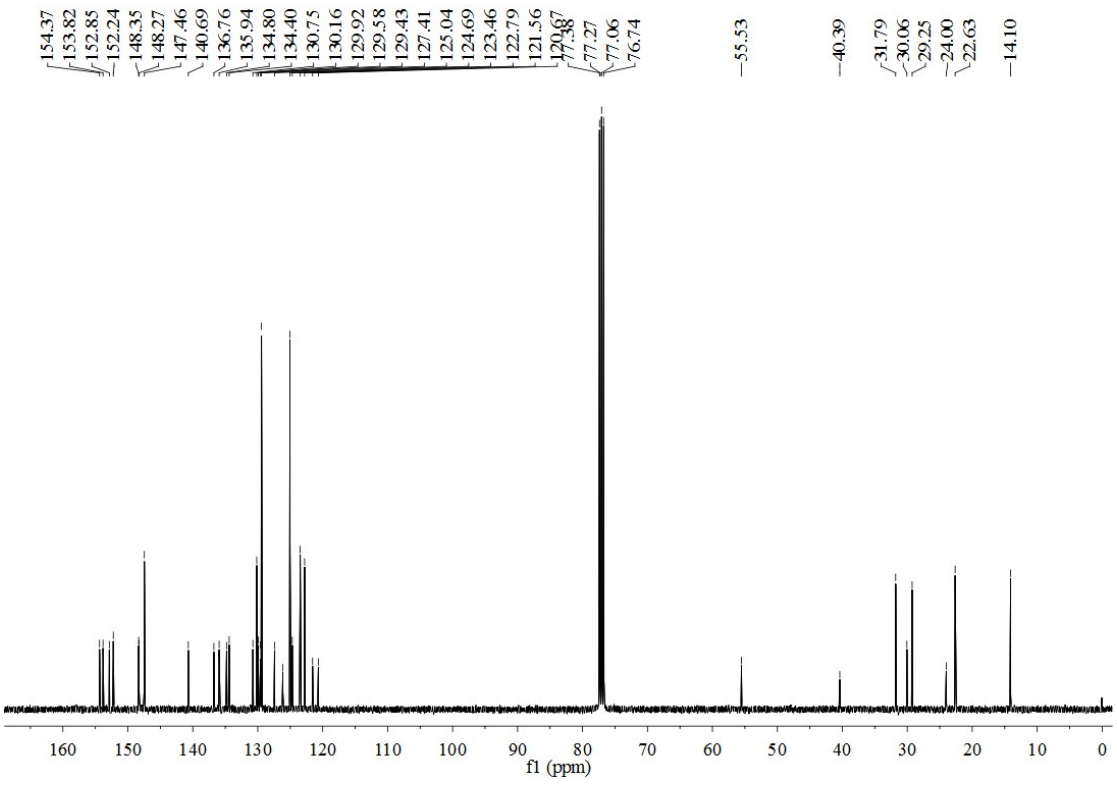

MS plot of TPA-BT-Br

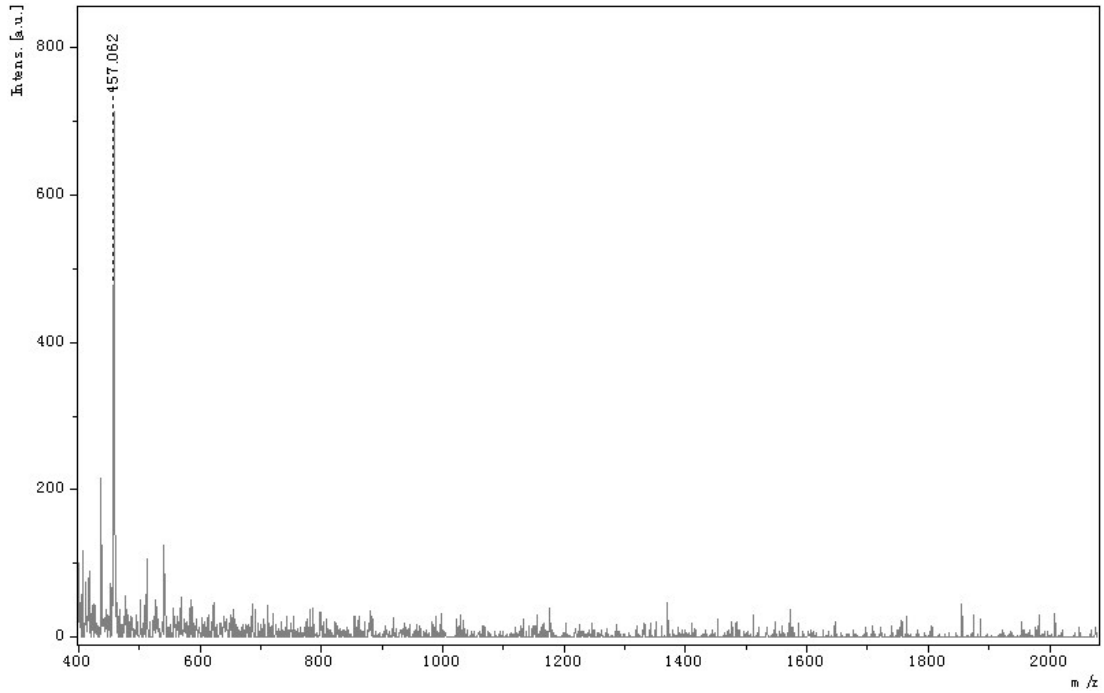

MS plot of TPA-BT-BPin

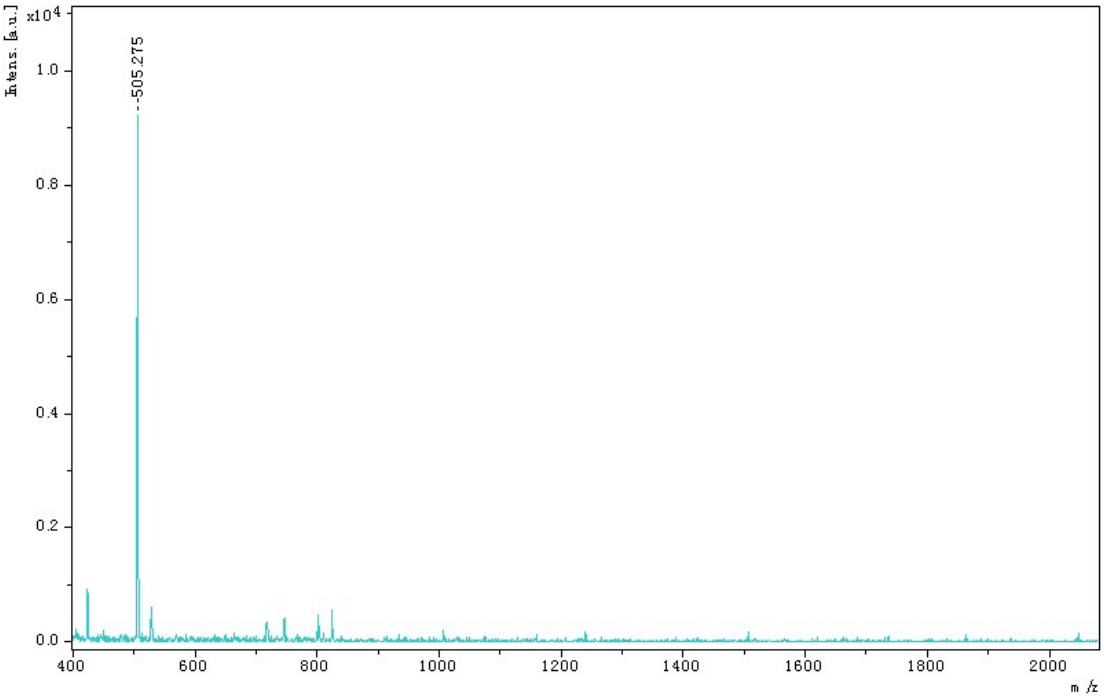

MS plot of TPA-BTPy

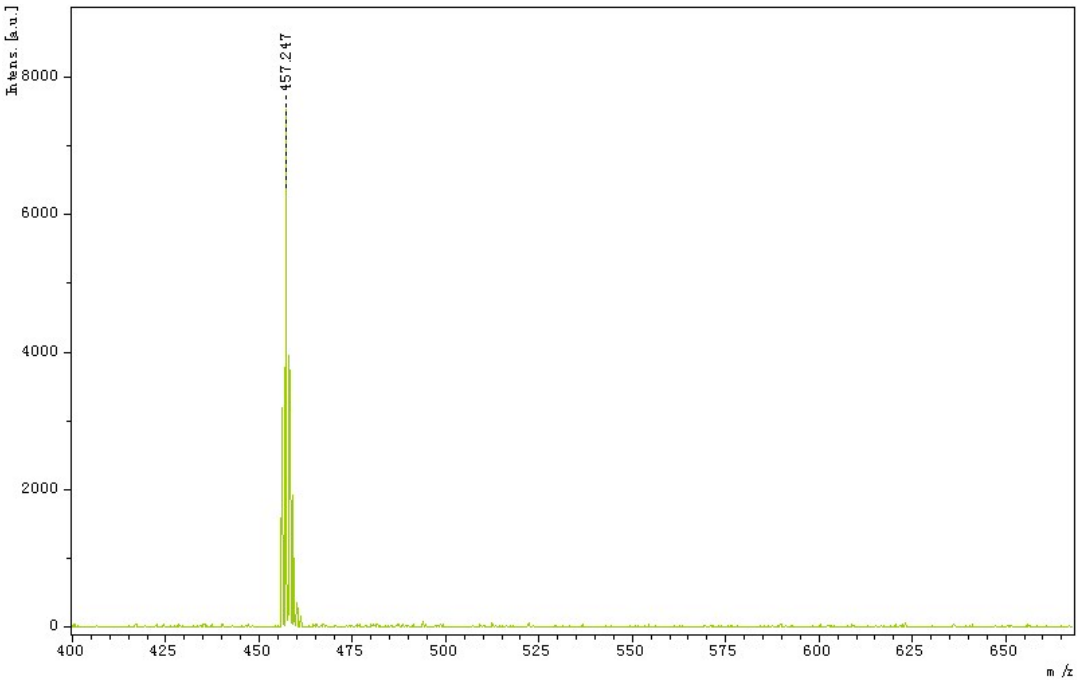

MS plot of TPA-BTPy-Br

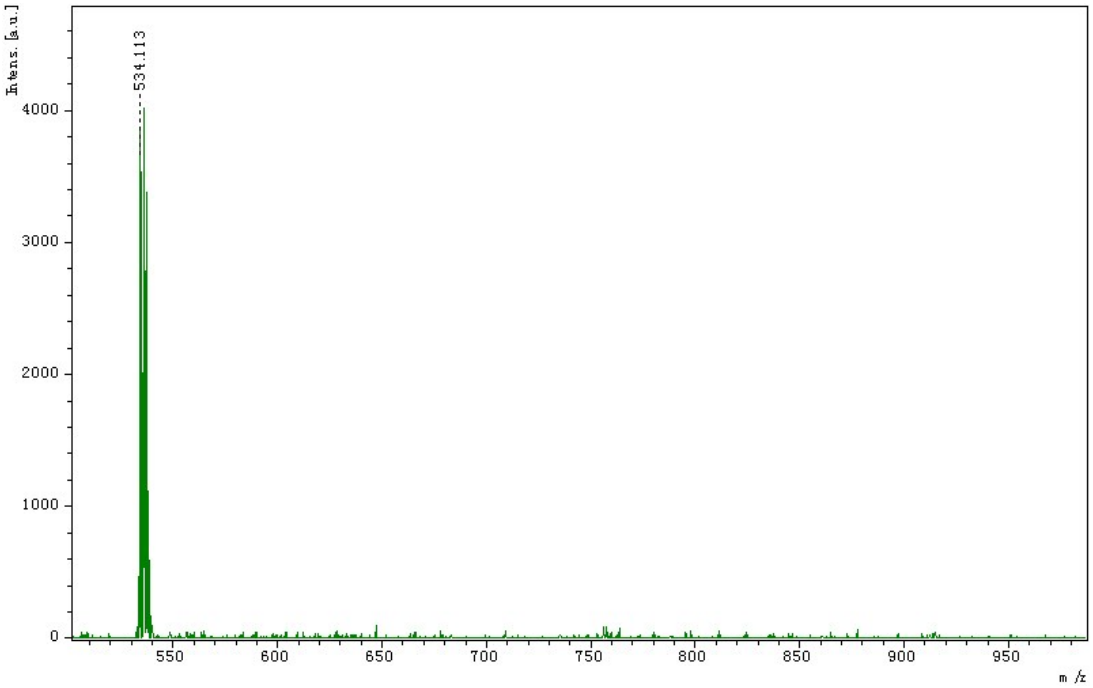

MS plot of TPA-BTPy-Fl

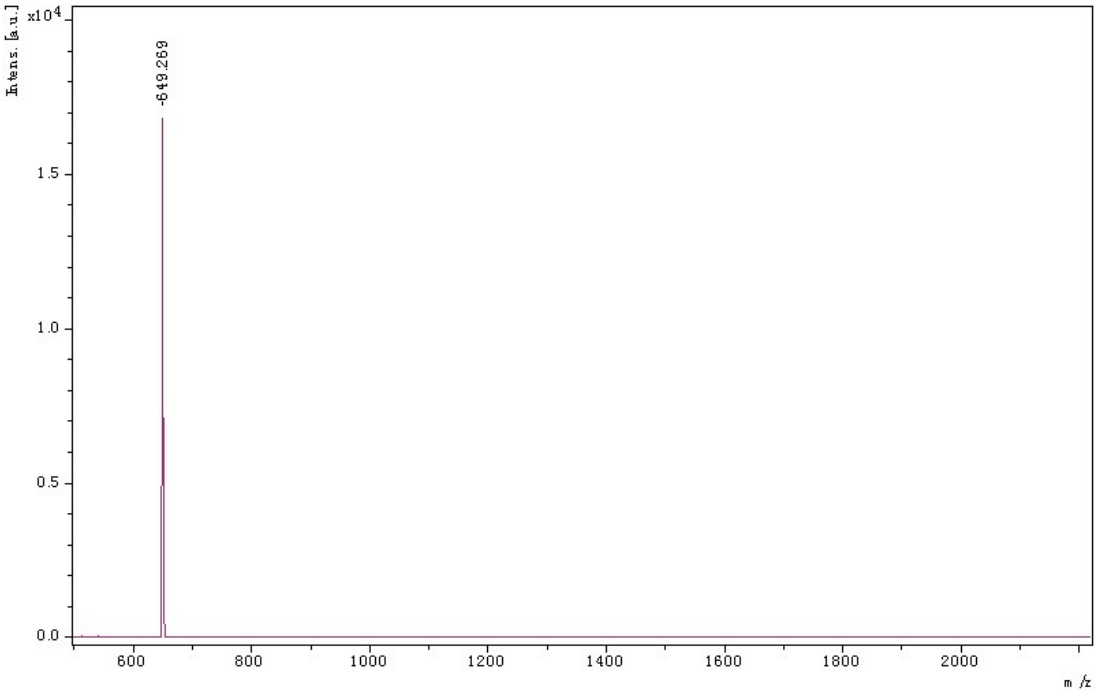

MS plot of Fl(TPA-BTPy)$_2$

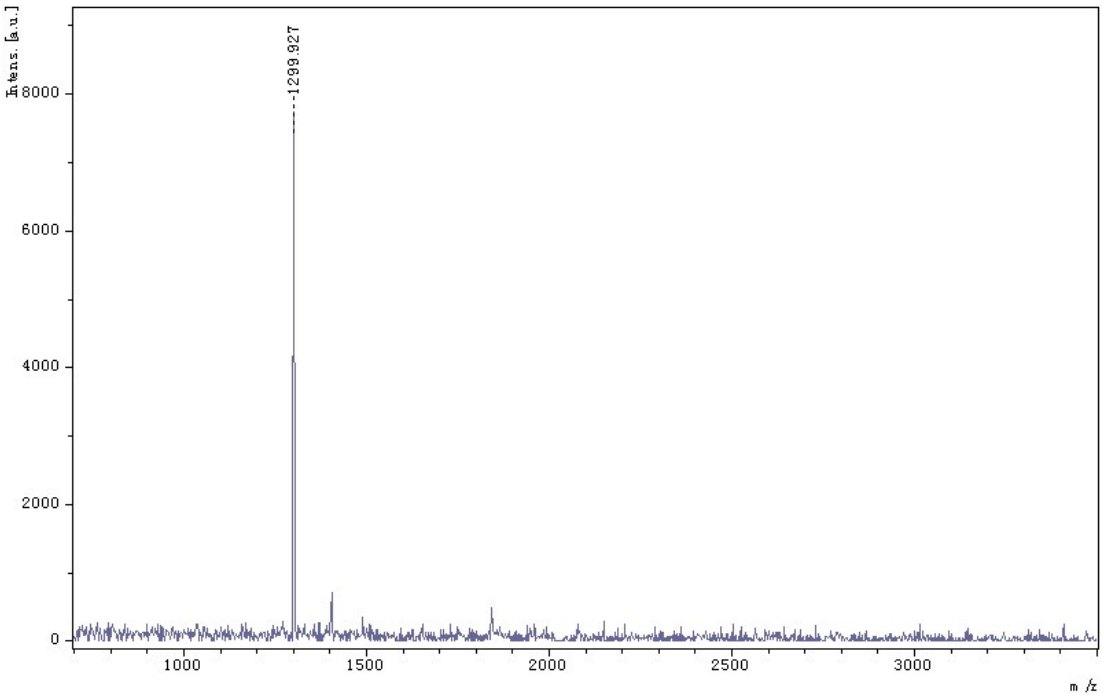

MS plot of (TPA-BTPy)Pt(pic)-Br

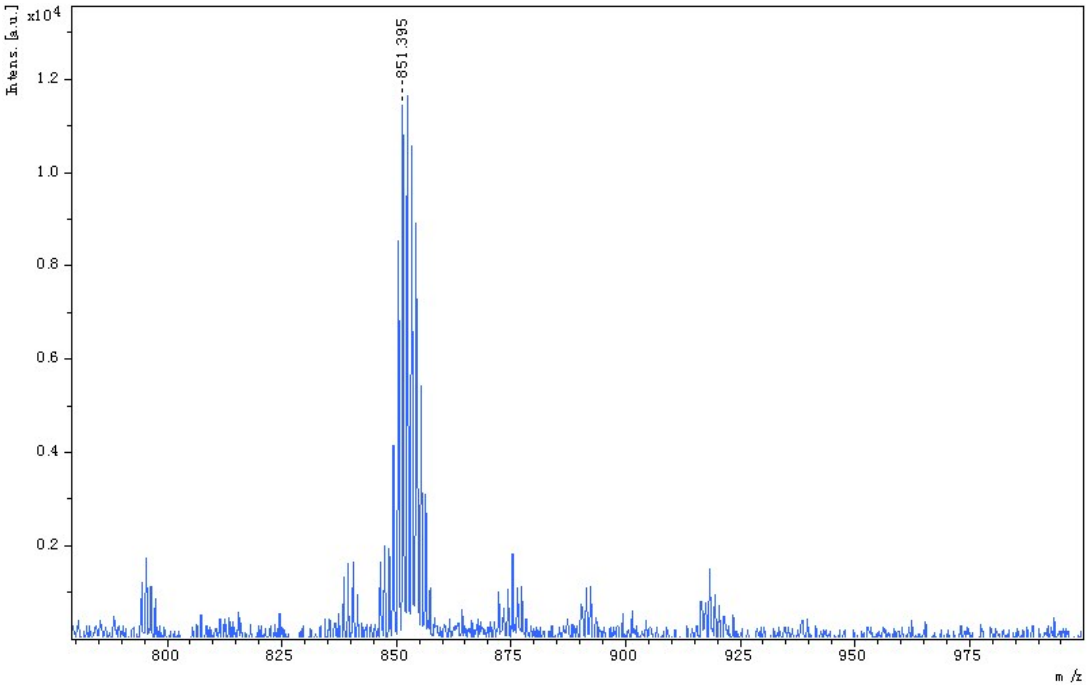

MS plot of (TPA-BTPy)Pt(pic)

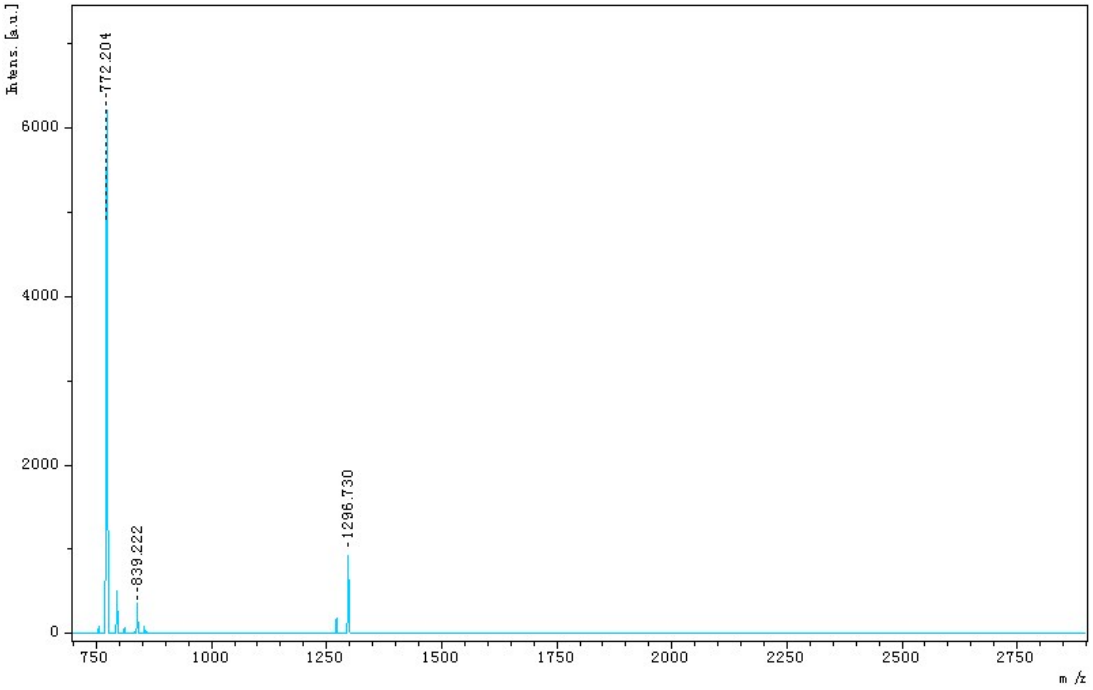

MS plot of (TPA-BTPy-Fl)Pt(pic)

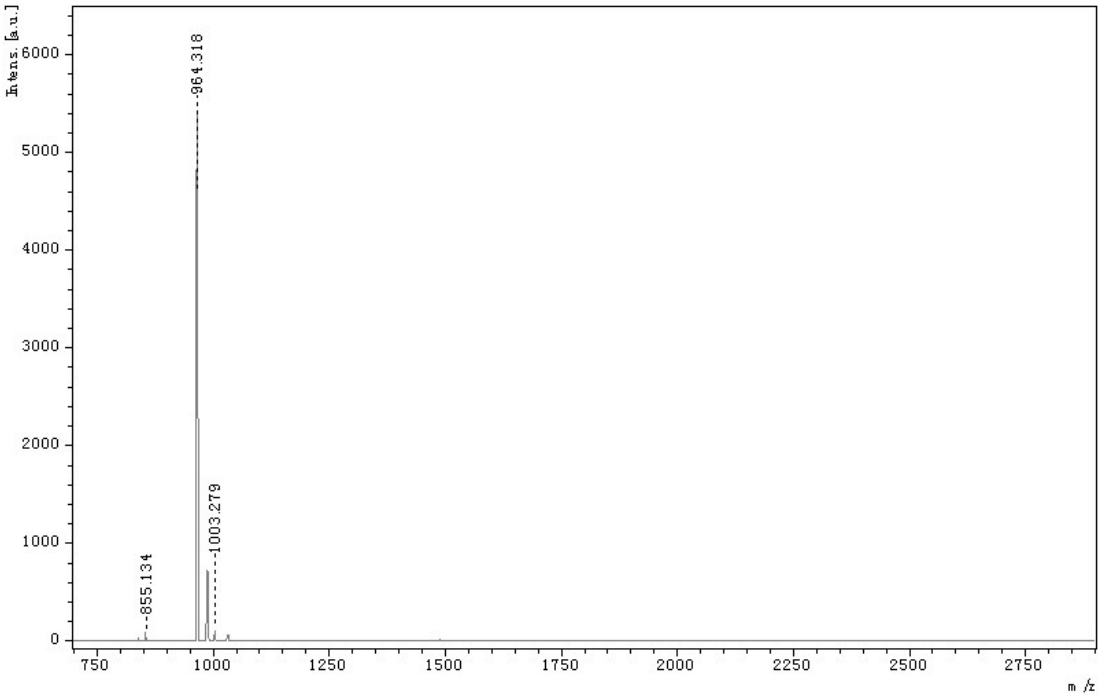

MS plot of [Fl(TPA-BTPy)$_2$] $Pt_2(pic)_2$